Available online at www.sciencedirect.com
ScienceDirect
Surface Science 600 (2006) 5084–5091
SURFACE SCIENCE
www.elsevier.com/locate/susc

One-dimensional structural and electronic properties of magnetite $Fe_3O_4(1\,1\,0)$

G. Maris *, O. Shklyarevskii, L. Jdira, J.G.H. Hermsen, S. Speller

Scanning Probe Microscopy, Institute for Molecules and Materials, Toernooiveld 1, Radboud University of Nijmegen, 6525 ED Nijmegen, The Netherlands

Received 12 April 2006; accepted for publication 27 August 2006
Available online 15 September 2006

Abstract

We study the structure and the electronic properties of the (1 1 0) surfaces of magnetite Fe_3O_4 thin films by scanning tunneling microscopy (STM) and spectroscopy (STS). The STM images show a surface reconstruction consisting of ridges along the $[\bar{1}\,1\,0]$ direction. Based on atomically resolved STM images we present a model for the observed ridge reconstruction of the surface, in agreement with a bulk-truncated layer containing both octahedral and tetrahedral iron ions. The metallic and semiconductor-like shapes of the measured current–voltage (I–V) curves indicate a non-uniform segregation of magnesium through the film. The weak contrast between the tops and valleys of ridges measured in the STS current maps is attributed to tetrahedral and octahedral coordination at the tops and the valleys, respectively. This attribution is in agreement with the proposed structure model. We observe a contrast enhancement at a tip change accompanied by a corrugation enhancement. This tip change is induced by picking up material from the sample, resulting in a magnetic tip. Thus, the contrast enhancement is attributed to detection of spin polarized current.

Keywords: Scanning tunneling microscopy; Iron oxide; Single crystal surfaces

1. Introduction

Magnetite (Fe_3O_4) is an interesting compound for both technological and fundamental reasons. Particularly, magnetite has a high potential for spin-valve and magnetic recording applications considering its high Curie temperature ($T_C \approx 850$ K) and the theoretically predicted 100% spin polarization [1–3]. In magnetic tunnel junctions, the tunneling magneto-resistance is related to the spin polarization and is maximal when the electrodes have 100% spin polarization. Taking in account its stability, its abundance in nature and the high degree of spin polarization, magnetite is a unique candidate in this respect.

In particular, the study of magnetite multilayers grown on insulating MgO has received a lot of attention due to the interest in understanding the magnetic coupling across a non-magnetic barrier for magnetic tunnel junction applications. MgO is an ideal substrate for epitaxy of Fe_3O_4, due to the small lattice mismatch: 0.33%. The quality of the surfaces and interfaces are key issues in developing magnetic devices. Thus, a good understanding of the relationship between the structural, magnetic and electronic properties down to atomic scale is of great importance. The use of scanning tunneling microscopy/spectroscopy (STM/STS) and spin-polarized STM/STS is crucial in this respect.

The (0 0 1) [4–8] and (1 1 1) [9–13] surfaces of magnetite have been extensively studied by STM both in single-crystal and thin-film forms and several surface terminations have been proposed. It has been shown for these orientations that the preparation conditions are crucial for the type of termination. Despite the efforts in studying the magnetite surfaces by STM, the STS investigations which give direct information about the density of states (DOS)

* Corresponding author. Tel.: +31 24 3653100; fax: +31 24 3652190.
E-mail address: g.maris@science.ru.nl (G. Maris).

0039-6028/$ - see front matter © 2006 Elsevier B.V. All rights reserved.
doi:10.1016/j.susc.2006.08.029

are still lacking. Furthermore, in comparison with the amount of effort in studying the (0 0 1) and (1 1 1) surfaces, little interest has been given to the (1 1 0) surface. STM investigations on this surface, in both thin film and single crystal form, show an one dimensional reconstruction and indicate a termination which consists of iron ions belonging to the two different magnetic sublattices [14,15]. Recently we observed on this surface a contrast in the current maps taken with a MnNi tip, which we attribute to magnetic origin [16].

In this paper, we present a detailed STM/STS study of the structural and electronic properties of the (1 1 0) surface of Fe_3O_4 thin films. Based on atomically resolved images, we derive a model for the surface reconstruction. The STS data are in concordance with the proposed model.

Magnetite has a face centered cubic (fcc) cubic inverse spinel crystal structure with a lattice constant of 8.397 Å [17]. The tetrahedral sites are occupied by Fe^{3+} ions and the octahedral sites are shared between equal amounts of Fe^{3+} and Fe^{2+} ions. The two sublattices formed by the octahedral and the tetrahedral sites couple antiferromagnetically and have different magnetic moments resulting in a net magnetization. For an oxide, magnetite has a relatively high conductivity at room temperature, e.g. 100 Ω^{-1} cm^{-1}. The conductance takes place at the octahedral sites due to the continuous hopping between Fe^{2+} and Fe^{3+} ions. Around 120 K the resistivity increases by a factor of ≈100. At this temperature, the so-called Verwey transition takes place. This transition is associated with the charge ordering at the octahedral sites. Due to the slight expansive strain of the epitaxial Fe_3O_4 films grown on MgO, the transition temperature in thin films is somewhat lower than observed for bulk Fe_3O_4 [18]. The sharpness and the temperature of the Verwey transition give indications for the crystallinity and phase purity of the magnetite films [19].

Two types of bulk termination for the (1 1 0) surface exist: type A contains both tetrahedrally and octahedrally coordinated Fe ions and type B contains octahedrally coordinated Fe ions (Fig. 1). The type A and type B layers alternate in the bulk with an interlayer spacing of 1.484 Å. The two types of surface are equally polar (+3 and −3) and thus assuming bulk truncations, the surface is expected to be reconstructed.

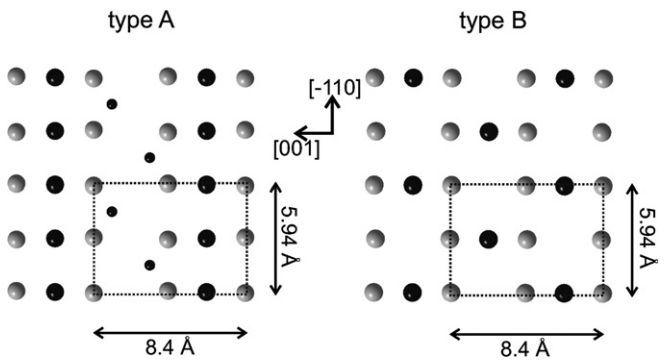

Fig. 1. A and B type (1 1 0) layers that alternate in bulk. The surface unit cell is indicated by a rectangle. Large grey circles denote O ions. The tetrahedral and octahedral Fe ions are represented as small and large black circles, respectively.

2. Experimental

The Fe_3O_4(1 1 0) thin films used in this study were deposited on MgO(1 1 0) substrates by e-beam evaporation from an Fe wire at a growth rate of 5 Å/min. The O pressure was 2×10^{-6} mbar and the substrate temperature during the evaporation was 523 K. Two different annealing procedures applied to separate films were used to obtain well-ordered surfaces. The first procedure consisted of 30 min annealing at 1000 K in ultrahigh vacuum (UHV). For the second procedure, a freshly grown film was annealed at 1000 K in 2×10^{-6} mbar oxygen followed by 10 min annealing at 1000 K in UHV. After preparation, the samples were transferred under UHV conditions in the analysis chamber. The samples were inspected by Auger electron spectroscopy (AES) to estimate the degree of contamination in the surface region. The AES spectra were acquired in the integral [$N(E)$] mode and were numerically differentiated. The composition in the surface region was estimated using atom sensitivity factors. The STM/STS measurements were performed at a base pressure below 5×10^{-11} mbar at room temperature with an Omicron UHV STM-1. For this study we have used about 20 paramagnetic W tips. Etched W tips were prepared by 15 min sputtering with Ar^+ ions (1 kV) and annealing at 700 K. This preparation resulted in sharp tips with a radius of approximatively 50 nm. Blunt (with radius >200 nm), clean W tips were subsequently obtained by melting their apex through electron bombardment (by applying 600 V between a W filament and the sharp tip placed 2 mm below the filament).

3. Results and discussion

3.1. Magnesium induced surface reconstruction

After the first preparation procedure consisting of annealing in UHV at 1000 K, the film showed a well-ordered surface showing ridges running along the [$\bar{1}$ 1 0] direction with a 25 Å periodicity corresponding to $p(1 \times 3)$ reconstruction [14,15]. The second procedure applied to a freshly grown film consisted of two steps. After the first step of annealing at 2×10^{-6} mbar at 1000 K a well-ordered surface was not obtained, although a tendency for this ordering could be distinguished. The ridge reconstruction was achieved after a second step of annealing at 1000 K in UHV.

From the Auger spectra (Fig. 2) of the annealed films we derive a contamination level for magnesium of ∼6%. This content of Mg^{2+} ions is sufficient to play an important role in the observed $p(1 \times 3)$ reconstruction. This is supported by a similar $p(1 \times 4)$ reconstruction observed on a (0 0 1) surface of a magnetite thin film grown on MgO after

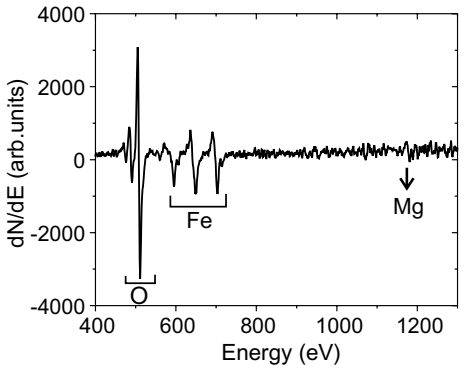

Fig. 2. AES spectrum showing the presence of Mg in the surface region.

annealing at 880 K [20], as well as on a natural magnetite single crystal after long annealing at 990 K [5,8]. In both cases, the reconstruction is interpreted as being induced by the contamination of the surface due to the segregation of Mg^{2+} and Ca^{2+} ions, respectively.

The reason that only a tendency for the ridge reconstruction was obtained after annealing in oxygen at 1000 K, while a clear ridge reconstruction was achieved by annealing in UHV at the same temperature is probably related to the balance between Fe, O and Mg ions necessary for a well-ordered surface. Presumably, when annealing is performed in O, a higher annealing temperature resulting in a higher Mg^{2+} concentration is necessary to obtain ridge reconstruction.

When annealing the Fe_3O_4 film grown on MgO, an interdiffusion of Mg and Fe cations takes place. This results in a substitution of the octahedrally coordinated Fe ions with Mg through the film. In order to determine weather this interdiffusion occurs only at the surface or through the entire thickness of the film, we have performed resistivity measurements on the film before and after annealing at 1000 K (Fig. 3). The measurements performed

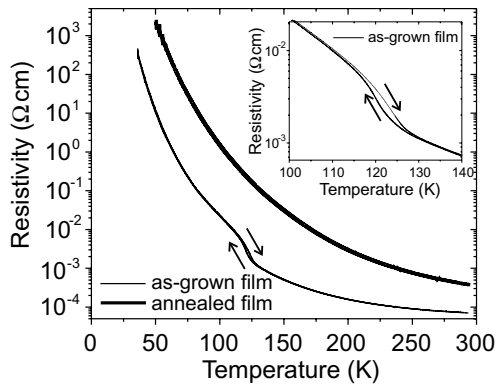

Fig. 3. Resistivity as a function of temperature measured in cooling down and warming up (arrows) of the 100 nm thick $Fe_3O_4(1\,1\,0)$ film grown on MgO. The Verwey transition at 121 K clearly seen in the as-grown film (thin line), vanishes for the annealed film (thick line). The inset shows the hysteresis in the phase transition region, as a result of finite speeds of cooling down and warming up.

before annealing show clearly the so-called Verwey transition at 121 K. The sharpness and the temperature of the Verwey transition give indications of a good crystallinity and phase purity of our magnetite films. After annealing at 1000 K, this phase transition disappears. The most plausible explanation is that the Mg^{2+} ions intercalate in the structure and decorate the octahedral iron rows resulting in a magnesium enriched Fe_3O_4 film, e.g. $Mg_xFe_{2+x}O_4$. This affects the Verwey transition associated with the charge ordering at the octahedral Fe sites.

Our STM images acquired with paramagnetic W tips show a surface morphology consisting of terraces with edges perpendicular to the $[\bar{1}\,1\,0]$ direction. The step heights between terraces are integer multiples of $3.0\,\text{Å} \pm 0.3\,\text{Å}$ [Fig. 4(a)]. This corresponds to the distance between similar layers (A–A or B–B) in the bulk structure. Each terrace ripples in the $[\bar{1}\,1\,0]$ direction. The periodicity of the ridges is mostly $25.0\,\text{Å} \pm 0.3\,\text{Å}$. This periodicity corresponds to threefold the bulk lattice constant (8.4 Å). Sometimes we observe a $34.0\,\text{Å} \pm 0.3\,\text{Å}$ periodicity in agreement with fourfold the bulk lattice constant. Shifts along the [0 0 1] direction with shift vectors of 1/2[0 0 1] are sometimes observed. The vertical corrugation perpendicular to the ridges varies between several tenths of pm and several hundreds of pm. As we will show later on in this paper, this variation is depending on the state of the tip, i.e., a pure W tip versus a modified W tip by picking up material from the sample.

In Fig. 4(b) we present an image showing well resolved double rows on top of each ridge and separated by 8.4 Å and one row in the middle of each valley. In this image we can distinguish as well a third row in between the two well resolved double rows on top of the ridges. These rows are running along the $[\bar{1}\,1\,0]$ direction. The average vertical corrugation is $0.75\,\text{Å} \pm 0.3\,\text{Å}$. Images taken with seven different W tips showed double rows on tops and single rows in the valleys. Sometimes, three or four rows can be distinguished on top of the ridges with distances varying between $4.0\,\text{Å} \pm 0.3\,\text{Å}$ and $12.0\,\text{Å} \pm 0.3\,\text{Å}$.

Using a very clean W tip obtained by melting its top through electron bombardment, we observe a significant improvement in the resolution of the STM images. In Fig. 5(a) we show an example of such an image where the top of one ridge with a width of $12.0\,\text{Å} \pm 0.3\,\text{Å}$ is very well resolved. This tip images periodicity along both the [0 0 1] and $[\bar{1}\,1\,0]$ directions. The smallest distance between two atoms imaged along the [0 0 1] direction is $2.1\,\text{Å} \pm 0.3\,\text{Å}$. This distance is in good agreement with the bulk Fe–O distance. Along the $[\bar{1}\,1\,0]$ direction, the periodicity is $3.0\,\text{Å} \pm 0.3\,\text{Å}$, which corresponds to the 2.97 Å distance between two consecutive oxygen ions or two consecutive octahedral iron ions of the bulk A layer (see Fig. 1). We attribute the indentation in the middle of the top of the ridge to the spacing between the tetrahedral Fe^{3+} ions rows of the bulk A-layer. This indented line feature is often resolved in our STM images using different W tips. The observed rows are attributed to octahedral iron rows and oxygen rows. The tetrahedral Fe^{3+} sites are sometimes

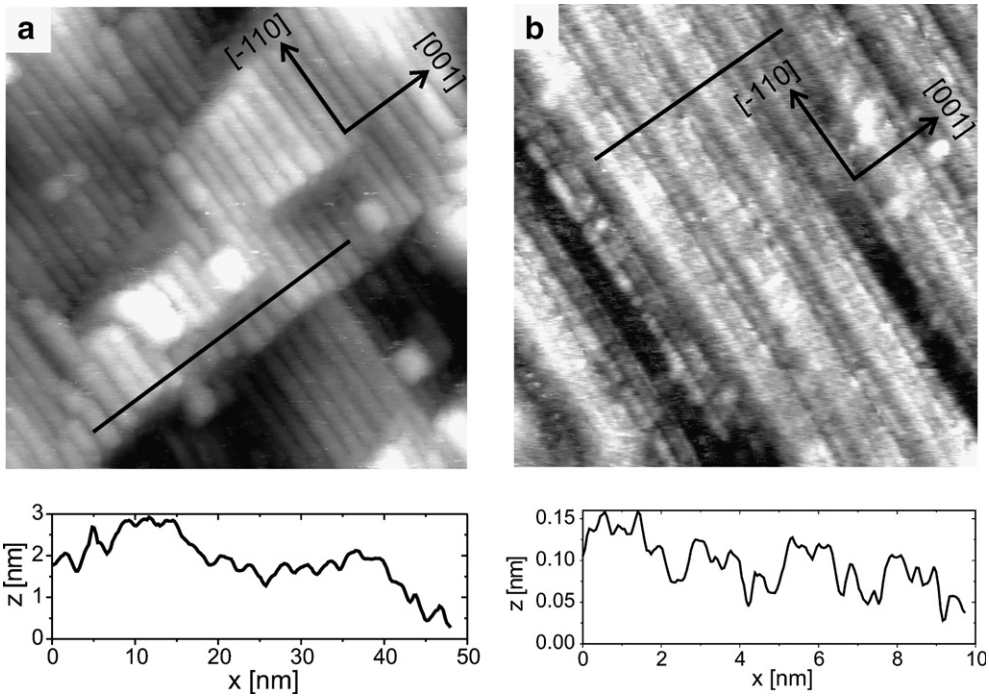

Fig. 4. (a) 700×700 Å^2 STM image showing terrace morphology with ridges along the $[\bar{1}10]$ direction separated by 25 Å. The image was taken with a W tip at a tunneling current of 0.85 nA and a bias voltage of 0.5 V. The line profile along the [001] direction shows the 25 Å periodicity of the ridges. (b) 200×200 Å^2 STM image showing resolution on tops and valleys of the ridges. The image was taken with a W tip at a tunneling current of 0.28 nA and a bias voltage of 1.5 V. The line profile along the [001] direction shows a 0.75 Å average vertical corrugation perpendicular to the ridges.

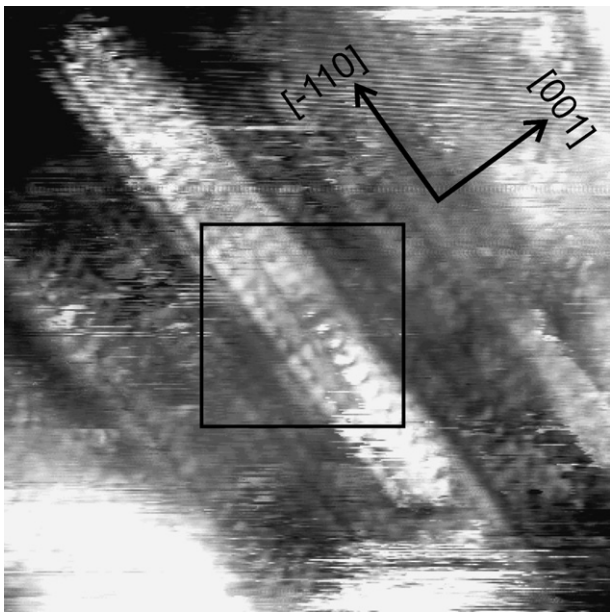

Fig. 5. 90×90 Å^2 atomically resolved STM image showing periodicity along $[\bar{1}10]$ and [001] directions. The image was acquired with a clean blunt W tip at a tunneling current of 0.76 nA and at a bias voltage of 1.5 V.

observed (in Fig. 6(a) such a site is indicated by an arrow). Although the valleys are less well resolved than the tops of the ridges, we can still identify in the valleys a 3.0 Å ± 0.3 Å periodicity along the $[\bar{1}10]$ direction corresponding to a bulk A layer.

Remarkably the sites of the oxygen atoms are imaged as bright features. This result contrasts with other STM studies on magnetite which report the oxygen atoms imaged as depressions [6,21]. Furthermore, the band structure calculations of bulk Fe_3O_4 indicate that the O(p) orbitals are lying well below the Fermi energy [1–3]. Although the situation for the surface can be different, the very large shift of more than 2 eV needed for the oxygen states to be accessible to tunneling electrons, is unlikely. However, the Mg^{2+} ions present at the surface can influence the position of the O(3s) orbitals. Indeed, electronic structure calculations show that the conduction band of MgO has predominantly O(3s) character [22]. Furthermore it was shown that in transition metal oxides like HfO_2, although the anion states are less important due to the presence of the metal d states, they are not negligible. Thus it is expected that the presence of Mg^{2+} ions in the $Mg_xFe_{2+x}O_4$ compound changes the character of the conduction band such that the O(3s) states play an important role. Based on this argument we can expect that in the vicinity of Mg^{2+} ions, the oxygen ions appear bright. While in this scenario, oxygen ions would appear as protrusions, the Mg^{2+} ions would appear as depressions. No depressions are visible in our STM images that could be attributed to the Mg^{2+} ions. Furthermore the A-type bulk layer has an excess of positive charge and the presence of the Mg^{2+} ions at the outermost layer would increase the surface charge and thus decrease its instability. In contrast, the presence of the Mg^{2+} ions at the subsurface, e.g. in the layer underneath the outermost layer will

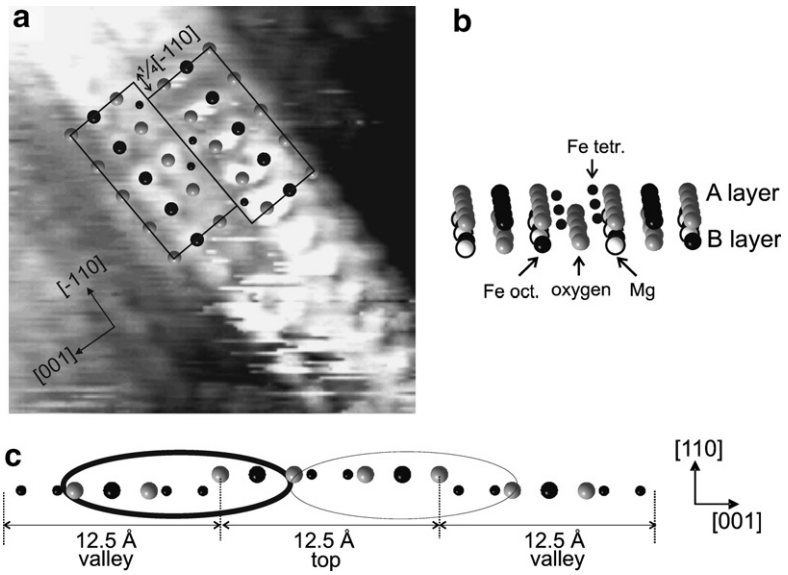

Fig. 6. (a) (30×30) Å^2 zoom in the area indicated by a square in Fig. 5(a). The image was acquired with a clean blunt W tip at a tunneling current of 0.76 nA and at a bias voltage of 1.5 V. On part of the STM topography we indicate atomic positions according to the model based on an A-type bulk layer. Large grey circles denote oxygen ions. The tetrahedral and octahedral Fe ions are represented as small black and large black circles, respectively. The rectangles represent the two sets of atoms that are shifted with a vector of $1/4[\bar{1}\,1\,0]$ in respect to their bulk positions. The arrow indicates an imaged atom corresponding to the tetrahedral Fe site. (b) The upper two layers side view of the model projected along the $[\bar{1}\,1\,0]$ direction. (c) The side view of the surface layer model projected along the $[\bar{1}\,1\,0]$ direction. By thick and thin ovals we highlight the regions of the current maps presented in Fig. 8 and corresponding to the bright and dark regions, respectively.

decrease the dipole moment perpendicular to the surface resulting in a more stable surface. Indeed, this subsurface layer is of B-type with an excess of negative charge and favors the intercalation of Mg^{2+} ions at the octahedral iron rows.

3.2. Surface model

The very well resolved images taken with blunt W tips allow us to suggest an atomic model of the top region of the ridges. Considering a bulk A-layer truncation, the imaged rows of atoms are attributed to octahedral Fe and O sites. In comparison to a bulk A-type truncation, the two sets of atoms highlighted by rectangles in Fig. 6(a) are shifted with respect to each other with a vector of $1/4[\bar{1}\,1\,0]$. Thus, on the basis of these well-resolved images we conclude that locally, the surface reconstruction is of the A type, containing both octahedral and tetrahedral Fe ions. The A truncated domains (highlighted by rectangles in Fig. 6(a)) are only ~6 Å wide and they are shifted with respect to each other. The side view of our structure model projected along the $[\bar{1}\,1\,0]$ direction is shown in Fig. 6(c). Note, that our model is based on bulk-truncation. Alternative models are thinkable if surface reconstruction and altered composition on the surface are included.

The most pronounced rows, commonly observed in our images, are double rows of protrusions separated by 8.4 Å on the top of each ridge and single rows of protrusions in the middle of each valley as in the image presented in Fig. 4(b). According to our model (Fig. 6(c)), these rows correspond to the octahedral iron sites rows. It is expected that the octahedral iron sites yield higher tunneling currents as these sites are responsible for conductivity in magnetite. Thus, the highest features are naturally attributed to the octahedral iron sites in concordance with our proposed model. The fact that with the blunt W tip we are able to resolve very well also the other species of atoms, i.e., tetrahedral Fe and oxygen is due to the high purity of this tip as a consequence of melting its top. The quality of melted W tips subsequently covered with a thin film of iron has been demonstrated in spin polarized STM measurements [23,24]. As the bulk A-layer is polar, charge neutrality can be obtained by vacancies at the tetrahedral sites. However, for a full description of a stable non-polar surface, the charges of the deeper layers have to be included.

In Fig. 6(b) we show the side view model of the upper two layers projected along the $[\bar{1}\,1\,0]$ direction. The Mg^{2+} ions intercalate at the subsurface B-layer in the interstitial positions in between two octahedral iron ions and influence the nearest neighbors oxygens of the outermost A-layer such that they appear as bright features. Note that the Fe–Fe spacing within the octahedral iron rows along the $[\bar{1}\,1\,0]$ direction of the B-layer is relatively large (6 Å) such that it is likely that the Mg^{2+} ions fit in between. The intercalation of the Mg^{2+} at the octahedral Fe rows ions is responsible for the disappearance of the Verwey transition upon annealing as observed in the resistivity measurements (see Fig. 3). Similar intercalation of the Ca^{2+} ions is proposed for the $p(1 \times 4)$ reconstructed (0 0 1) surface of an Fe_3O_4 natural crystal [8].

Another explanation which sustains that the observed $p(1 \times 3)$ reconstruction is induced by the Mg impurities is

based on surface energy principles according to which, the presence of the positive ions at the surface results in a coarsening of the surface in contrast to a less coarse surface favorable in the presence of negative ions. Thus, the electropositive species lead to coarsening of a conductive surface while electronegative adsorbates rather lead to decoarsening.

The location of the Mg^{2+} ions at the subsurface agrees as well with the AES results. For high energies of the Auger transition, like the one corresponding to the observed magnesium peak, the escape depth is a couple of nanometers and thus this peak can well originate from the Mg^{2+} ions located at the subsurface.

3.3. Electronic properties of the surface

The conductivity characteristic of the $Fe_3O_4(1\,1\,0)$ surface is analyzed by STS. Two types of shape for the *I–V* characteristics are observed in the STS measurements performed with the W tips. The majority of measurements show semiconductor-like *I–V* curves also at low tunneling resistances (corresponding to 2 nA tunneling current and 1 V gap voltage) (Fig. 7). However, approximately 10% of the time we have observed ohmic-like shapes for the *I–V* curves. As ohmic-like *I–V* characteristics have been observed with the very clean W tip obtained by melting its top, we have speculated at first that the purity of the tip influences the type of shape for the *I–V* curves. However, new experiments excluded this possibility as with the same standard prepared W tip we measured both types of shapes in different regions of the sample. We believe that the difference in the *I–V* shape is related to the non-uniform segregation of Mg through the film [20]. Thus, regions with lower concentration of Mg ions can still show metallic-like shapes for the *I–V* curves, while regions with a larger concentration of Mg will have a lower conductivity and will show semiconductor-like shapes for the *I–V* curves.

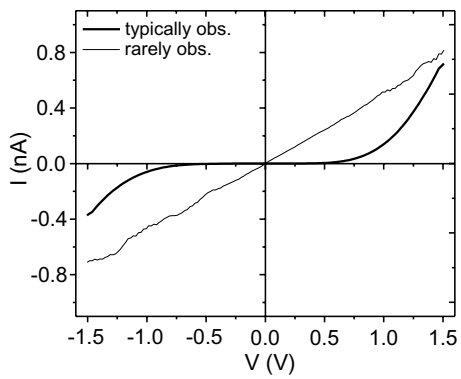

Fig. 7. Typically semiconductor-like and rarely observed ohmic-like shapes of the *I–V* curves on top and on valleys of ridges. As the *I–V* curves taken in the valleys and on the tops of the ripples differ only insignificantly, we show the *I–V* curves obtained by averaging over both valley and top areas. The tip-sample distance was set by stabilizing a tunneling current of 0.73 nA and 0.65 nA and a bias voltage of 1.5 V and 1.5 V for the semiconductor and ohmic-like curves, respectively.

In Fig. 8(a) and (b) we present the derivatives of the *I–V* curves measured on top and in the valleys of the ridges in the second and third measurements of a sequence of four consecutive STS measurements. This sequence is collected in the region presented in Fig. 4(b). The topography images are shown in the left inset of Fig. 8(a) and (b). The current maps at 1.06 V bias voltage is presented in the right inset of Fig. 8(a) and (b). For the first two measurements the top-valley corrugation in the topography had an average value of 0.75 Å (see Fig. 4(b)) and very small contrast has been observed in the corresponding current map. The same situation is observed for a part (below the arrow in Fig. 8(b)) of the third measurement. At one point indicated by an arrow in Fig. 8(b) the state of the tip has changed resulting in changes in both topography and current map (the part of the image above the arrow in Fig. 8(b)). Thus at the tip change, the top-valley corrugation increases to an average value of 3.5 Å and the octahedral iron sites rows in the valleys are not anymore visible, i.e., the valleys are imaged dark. In the current map we observe an increased contrast associated with the ripple structure. Furthermore, the current measured on tops and valleys becomes weaker. This situation is maintained also for the fourth measurement.

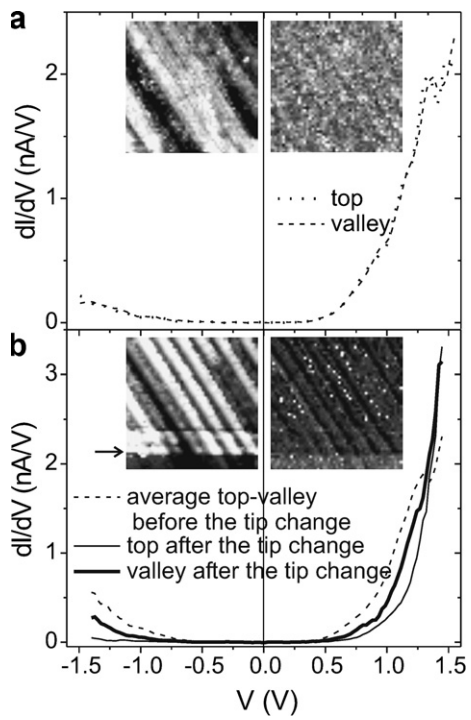

Fig. 8. (a) and (b) Derivatives of the *I–V* curves obtained on the tops and the valleys of the ridges in two consecutive STS measurements. Each curve is the average over approximately hundred single curves. Inset: 200×200 Å^2 STM image and corresponding current map. The bias voltage for these maps is 1.06 V. The tip sample distance was set by stabilizing a tunneling current of 1 nA and a bias voltage of 1.5 V. The arrow in (b) indicates the change of the tip state. The scanning has been acquired in the upwards direction.

By superimposing the current map on the topography image, a slight shift is observed, such that the brighter zones (higher conductance) in the current map correspond to the main part of the valley and a small part of the top in topography, while the darker zones (lower conductance) correspond to the main part of the tops and a small part of the valleys. In the topography model presented in Fig. 6(c) we highlight by the thick and thin ovals the regions corresponding to the bright and dark regions in the current map. For practical reasons, these regions will be referred in the following as corresponding to valleys and tops of the ridges.

According to the model presented in Fig. 6(c), the top of the ridges are dominated by the tetrahedrally coordinated iron, while the valleys are dominated by the octahedrally coordinated iron. This explains the small contrast typically observed in the current maps acquired with W tips. Furthermore, as the octahedral sites are responsible for the conduction mechanism in magnetite, the always observed higher conductance in the valleys agrees with the dominating octahedral coordination of our model. In magnetite, the octahedral and the tetrahedral sublattices have antiparallel orientations of the magnetic moments. Based on our proposed model, the octahedral character of the valleys and the tetrahedral character of the tops result in an antiparallel orientation of the magnetization vectors on tops and valleys. When using a magnetic tip, the detection of the spin polarization component results in an enhanced contrast in the current map and an enhanced corrugation in the topography between tops and valleys due to their antiparallel oriented magnetization directions.

A plausible explanation for the change of the W tip state (see arrow Fig. 8(b)) refers to a soft crash of the tip during the STS measurements when the tip picked up material from the film. Thus, hereby the tip is rendered spin selective to certain degree. The detection of the spin polarized contribution to the tunneling current leads to a corrugation enhancement and a stronger appearance of the top-valley contrast in the current map, as observed above the arrow in Fig. 8(b). By picking up magnetite, the tip-sample separation becomes smaller. Furthermore, due to the presence of magnetite on its top, the modified W tip becomes less conductive. This explains the lower conductivity measured on tops and valleys compared to the conductivity measured before the tip change.

4. Conclusions

The STM study on a magnetite (1 1 0) surface indicates a morphology consisting of terraces that ripple in the $[\bar{1}\,1\,0]$ direction. The AES and resistivity measurements indicate the segregation of Mg^{2+} through the entire thickness of the film. Atomically resolved images taken with a clean blunt W tip resolves periodicity in $[\bar{1}\,1\,0]$ and [0 0 1] directions. Based on these images we build a model in agreement with a bulk A-type layer containing both octahedral and tetrahedral Fe ions. The Mg^{2+} ions intercalate at the interstitial positions of the octahedral iron rows in the B-type layers. This is in agreement with both AES spectra and the resistivity measurements.

In the STS measurements we observe two types of I–V characteristics: ohmic-like and semiconductor-like. Our data suggest that this is related to a non-uniform Mg^{2+} segregation through the film resulting in regions with different conductivities. The majority of the measured I–V curves maintain a semiconductor-like shape down to low tunneling resistances. A small contrast between the tops and valleys of the ripples is typically observed in the current map. This contrast is attributed to the tetrahedral and octahedral character of the tops and the valleys, respectively, in agreement with the proposed model. We observe a contrast enhancement at the W tip change accompanied by a corrugation enhancement. This tip change can be caused by picking up material from the sample, resulting in a magnetic tip. The detection of the spin polarization component to the tunneling current explains the observed contrast enhancement.

Acknowledgements

The authors would like to thank Professor R.A. de Groot for helpful discussions. This work was supported by the ASPRINT European project (NMP-CT-2003-001601) and by NanoNed, the Dutch nanotechnology programme of the Ministry of Economic Affairs.

References

[1] A. Yanase, N. Hamada, J. Phys. Soc. Jpn. 53 (1984) 312.
[2] A. Yanase, N. Hamada, J. Phys. Soc. Jpn. 68 (1999) 1607.
[3] Z. Zhang, S. Satphaty, Phys. Rev. B 44 (1991) 13319.
[4] J.M. Gaines, P.J.H. Bloemen, J.T. Kohlhepp, C.W.T. Bulle-Lieuwma, R.M. Wolf, A. Reinders, R.M. Jungblut, P.A.A. van der Heijden, J.T.W.M. Eemeren, J. aan de Stegge, W.J.M. de Jonge, Surf. Sci. 373 (1997) 85.
[5] C. Seoighe, J. Naumann, I.V. Shvets, Surf. Sci. 440 (1999) 116.
[6] B. Stanka, W. Hebenstreit, U. Diebold, S.A. Chambers, Surf. Sci. 448 (2000) 49.
[7] S.A. Chambers, S. Thevuthasan, S.A. Joyce, Surf. Sci. Lett. 450 (2000) L273.
[8] S.F. Ceballos, G. Mariotto, K. Jordan, S. Murphy, C. Seoighe, I.V. Shvets, Surf. Sci. 548 (2004) 106.
[9] S. Murphy, A. Cazacu, N. Berdunov, I.V. Shvets, Y.M. Mukovskii, J. Magn. Magn. Mater. 290–291 (2005) 201.
[10] N. Berdunov, S. Murphy, G. Mariotto, I.V. Shvets, Phys. Rev. Lett. 93 (2004) 057201.
[11] A.R. Lennie, N.G. Condon, F.M. Leibsle, P.W. Murray, G. Thornton, D.J. Vaughan, Phys. Rev. B 53 (1996) 10244.
[12] W. Weiss, M. Ritter, Phys. Rev. B 59 (1999) 5201.
[13] Sh.K. Shaikhutdinov, M. Ritter, X.G. Wang, H. Over, W. Weiss, Phys. Rev. B 60 (1999) 11062.
[14] R. Jansen, V.A.M. Brabers, H. van Kempen, Surf. Sci. 328 (1995) 1783.
[15] R. Jansen, R.M. Wolf, H. van Kempen, J. Vac. Sci. Technol. B 14 (1996) 1173.
[16] G. Maris, L. Jdira, J.G.H. Hemrsen, S. Murphy, G. Manai, I.V. Shvets, S. Speller, J. Phys. Soc. Jpn. 45 (3B) (2006) 2225.
[17] R.W.G. Wyckoff, second ed.Crystal Structures, vols. 1–3., Krieger, Malabar, 1982.

[18] D.S. Lind, S.D. Berry, G. Chern, H. Mathias, L.R. Testardi, Phys. Rev. B 45 (1991) 6218.
[19] J.J. Krebs, D.S. Lind, S.D. Berry, J. Appl. Phys. 73 (1993) 6457.
[20] J.F. Anderson, M. Kuhn, H. Diebold, K. Shaw, P. Stoyanov, D. Lind, Phys. Rev. B 56 (1997) 9902.
[21] G. Mariotto, S. Murphy, I.V. Shvets, Phys. Rev. B 66 (2002) 245426.
[22] P.K. Boer, R.A. de Groot, J. Phys: Condens. Matter 10 (1998) 10241.
[23] T.K. Yamada, M.M.J. Bischoff, G.M.M. Heijnen, T. Mizoguchi, H. van Kempen, Phys. Rev. Lett. 90 (2003) 056803.
[24] A. Kubetzka, P. Ferriani, M. Bode, S. Heinze, G. Bihlmayer, K. von Bergmann, O. Pietzsch, S. Blügel, R. Wiesendanger, Phys. Rev. Lett. 94 (2005) 087204.